

Experimental Study and Detailed Modeling of Toluene Degradation in a Low-Pressure Stoichiometric Premixed CH₄/O₂/N₂ Flame[†]

A. El Bakali,*[‡] L. Dupont,[‡] B. Lefort,[‡] N. Lamoureux,[‡] J. F. Pauwels,[‡] and M. Montero[§]

Physicochimie des Processus de Combustion et de l'Atmosphère, UMR CNRS 8522 PC2A, Université des Sciences et Technologies de Lille, 59655 Villeneuve d'Ascq Cedex, France, and Direction de la Recherche, Gaz de France, B.P. 33, 93211 Saint Denis La Plaine Cedex, France

Received: October 28, 2006; In Final Form: January 8, 2007

Temperature and mole fraction profiles have been measured in laminar stoichiometric premixed CH₄/O₂/N₂ and CH₄/1.5% C₆H₅CH₃/O₂/N₂ flames at low pressure (0.0519 bar) by using thermocouple, molecular beam/mass spectrometry (MB/MS), and gas chromatography/mass spectrometry (GC/MS) techniques. The present study completes our previous work performed on the thermal degradation of benzene in CH₄/O₂/N₂ operating at similar conditions. Mole fraction profiles of reactants, final products, and reactive and stable intermediate species have been analyzed. The main intermediate aromatic species analyzed in the methane–toluene flame were benzene, phenol, ethylbenzene, benzylalcohol, styrene, and benzaldehyde. These new experimental results have been modeled with our previous model including submechanisms for aromatics (benzene up to *p*-xylene) and aliphatic (C1 up to C7) oxidation. Good agreement has been observed for the main species analyzed. The main reaction paths governing the degradation of toluene in the methane flame were identified, and it occurs mainly via the formation of benzene (C₆H₅CH₃ + H = C₆H₆ + CH₃) and benzyl radical (C₆H₅CH₂ + H = C₆H₅CH₂ + H₂). Due to the abundance of methyl radicals, it was observed that recombination of benzyl and methyl is responsible for main monosubstitute aromatic species analyzed in the methane–toluene flame. The oxidation of these substitute species led to cyclopentadienyl radical as observed in a methane–benzene flame.

1. Introduction

Aromatics are well-known to be harmful for health and environment due to their toxicity and because their oxidation can form toxic species. Aromatic compounds are largely used as solvents and added in a significant portion to most practical fuels like kerosene and diesel.¹ Moreover, benzene and substituted aromatics are frequently found in both automobile exhaust and evaporative emission. It is largely agreed that small aromatics are precursors of polycyclic aromatic hydrocarbons (PAHs), which are well-known for their mutagenicity and carcinogenicity.² While significant investigations have been reported for high temperature of aliphatic hydrocarbons, fewer studies are available for aromatic compounds.³ Moreover, the available investigations have been largely focused on the oxidation of the pure aromatic compounds, whereas they are present in practical fuels with other hydrocarbon species, mainly with alkanes.

The first objective of this work is to reproduce experimental data for alkanes/aromatics oxidation in premixed flame conditions. The second objective is to propose a detailed mechanism able to produce the experimental data. Our recent previous articles reported numerical and experimental investigations for low-pressure stoichiometric methane/1.5% benzene/air flame and methane/air flame.^{4,5} The thermal decomposition of benzene in methane flame has been discussed in ref 4, and a reaction kinetic model was proposed. This model has been recently extended

to the low-temperature oxidation of benzene/*n*-heptane/O₂/Ar mixtures to simulate ignition delay times obtained in a large range of pressure in a rapid compression machine.⁵ We report here new experimental results obtained in methane/oxygen/nitrogen and methane/1.5% toluene/oxygen/nitrogen flames which have been studied under conditions similar to that of methane–benzene flame.

2. Toluene Oxidation: Literature Investigations

The majority of the investigations conducted on toluene oxidation were limited to the global data: ignition delays in shock tube^{6,7} or in rapid compression machine⁸ and laminar flame speeds.^{9,10} These first studies helped in establishing the first chemical kinetic mechanisms for benzene and toluene oxidation. Species mole fraction profiles reported have been obtained in turbulent flow reactor or in jet stirred reactor^{11–15} at atmospheric pressure.

The first model of toluene oxidation has been proposed by McLain et al.¹⁶ by modeling their experimental mole fraction profiles obtained in shock tube. The model of McLain derives from investigations of Asaba and Fujii¹⁷ and Fujii and Asaba.¹⁸ On the basis of the qualitative kinetic scheme outlined by Brezinsky,¹³ Bittker proposed a detailed kinetic model for benzene and toluene oxidation¹⁹ which has been updated²⁰ in 1991 to better predict phenol mole fraction measured by Lovell et al.²¹ Bittker²⁰ assigned to the reaction of consumption of phenol with OH radical a rate constant five times higher than the constant reported by He et al.²² Due to this change and to the incorporation of new measured rate constants, a reasonable agreement has been observed between the model and the experimental species concentrations of Lovell et al.²¹ obtained

[†] Part of the special issue "James A. Miller Festschrift".

* To whom correspondence should be addressed. E-mail: abderrahman.el-bakali@univ-lille1.fr. Phone: (33)-3-20434804. Fax: (33)-3-20436977.

[‡] Université des Sciences et Technologies de Lille.

[§] Gaz de France.

TABLE 1: Initial Composition of Stoichiometric Low-Pressure Premixed Methane and Methane–Toluene Flames

	%CH ₄	%C ₆ H ₅ CH ₃	%O ₂	%N ₂
reference flame	11.1	0.0	22.2	66.7
flame CH ₄ /1.5%C ₆ H ₅ CH ₃	4.9	1.5	23.4	70.2

in turbulent flow reactor. However, Bittker's model²⁰ overestimates the ignition delay times measured by Burcat in shock tube.⁷

The mechanism of Emdee et al.,¹⁴ known in the literature as the EBG model, consists of 130 reactions instead of 120 reactions in the case of Bittker's model. In addition to the abstraction reaction from toluene by O₂, Emdee includes the addition of the molecular oxygen reaction. The mechanism of Emdee is the reference for the most recent models reported for the oxidation of benzene and toluene. It is based on the qualitative mechanism proposed by Brezinsky¹³ for toluene oxidation, which attributes to the phenyl radical a significant role in the ring destruction. Phenyl yields phenoxy radical which undergoes a contraction expelling CO and cyclopentadienyl radical. Emdee verified his model against Lovell's data.²¹ As observed with Bittker's mechanism, large discrepancies have been observed for phenol, cyclopentadiene, and carbon monoxide. Emdee attributed these disagreements to the uncertainties on the small molecules and did not suspect the first steps of toluene oxidation. Bittker²³ published a new version of his toluene model including the submechanism of toluene proposed by Emdee et al.¹⁴ The reviewed mechanism was not able to fit the turbulent flow data obtained in the rich conditions.¹¹ In 1998, Klotz et al.²⁴ published an update of the EBG model, including 97 species and 529 reactions. This model, known as the KBG model, was proposed to simulate stable mole fraction profiles measured for neat toluene oxidation, for neat *n*-butane oxidation, and for *n*-butane/toluene oxidation in flow reactor at 1 atm. Pitz et al.²⁵ proposed a detailed kinetic reaction mechanism for combustion of toluene. The model of Pitz combines the mechanism of Zhong and Bozzelli²⁶ and C1–C4 submechanism oxidation of Curran et al.²⁷ with a more accurate description for the reaction of benzyl with molecular oxygen based on the Bozzelli et al. study.²⁸ The authors verified their model against shock tube and flow reactor data.

A more detailed mechanism has been published for the oxidation of toluene in a jet stirred reactor at atmospheric pressure by Ristori et al.,¹⁵ which is strictly identical to the model published by Dagaut et al.²⁹ 1 year after. More recently, Sivaramakrishnan et al.³⁰ evaluated KBG and Dagaut models against mole fraction profiles of stable species obtained for the oxidation of toluene at very high pressure range (22–550 bar) under stoichiometric and rich conditions. Both models exhibited large discrepancies. The authors identified nine elementary reactions by using reaction path analysis and sensitivity analysis. The adjustment of the rate coefficients of these reactions and the addition of nine reactions led to better agreement between the modified KBG mechanism and experiments.

According to our literature review, all the above-mentioned literature models have been validated in reactor conditions (jet stirred reactor, flow reactor, and shock tube). The mechanism reported by Lindstedt and Maurice³¹ for benzene and toluene oxidation is the only one that has been evaluated in flame conditions. In their 141 species, 743 reactions mechanism, the authors proposed additional routes for the destruction of the aromatic ring and cyclopentadiene which are more probable to occur in flame conditions. The model has been validated in a wide range of combustion regime, including not only flow

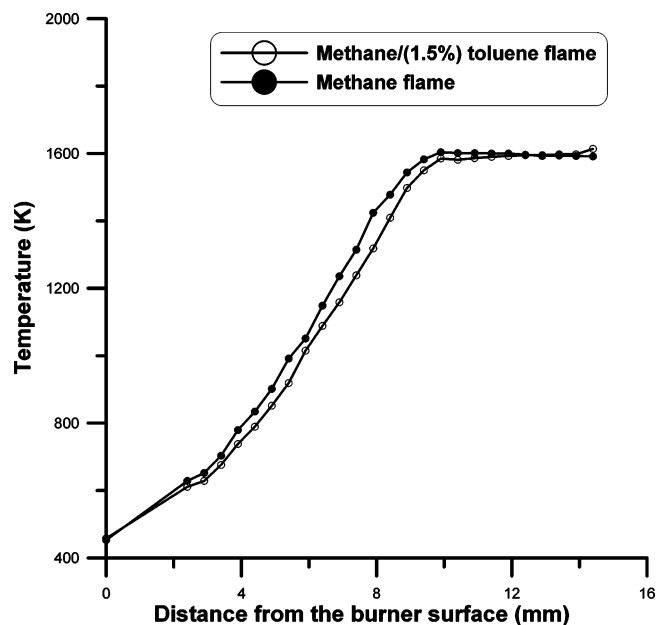


Figure 1. Temperature profiles measured in CH₄/O₂/N₂ (open symbols) and CH₄/1.5%C₆H₅CH₃/O₂/N₂ (full symbols) flames at 0.0519 bar. $\phi = 1.0$.

reactors and shock tubes but also premixed flames and counter flow diffusion flames. Compared to the predictions of literature mechanisms, the model of Lindstedt and Maurice³¹ exhibited the best agreement with our methane/BTX (benzene, toluene, *p*-xylene) low-pressure experimental results and then was selected as the starting point for the present modeling work. On the other hand, due to the lack of experimental data in toluene/alkanes mixtures, except KBG model (in flow reactor conditions), the validation of the above-discussed models has been limited to the oxidation of the neat fuel (neat alkanes oxidation or neat toluene oxidation) at atmospheric pressure and detailed experimental fraction profiles have been limited to moderate temperature range (<1400 K). Shandross et al.³² evaluated three literature models^{14,33,34} against experimental results obtained in a low-pressure stabilized flame of hydrogen/oxygen/argon mixture seeded with benzene; the three models tested exhibited large discrepancies for fuel blends, whereas they show good agreements for the neat fuels. In flame conditions there is a real lack of data even in the case of neat toluene oxidation. Only one literature experimental study has been found and concerned non-premixed toluene flame.³⁵ To address this lack of data essential for development mechanism for the oxidation aromatic/alkanes mixtures, our laboratory carried out series of experimental and numerical investigations in laminar low-pressure premixed methane flame with and without 1.5% of BTX under similar conditions. This work represents the first experimental results in premixed low-pressure methane–toluene flame. The study complements our previous experimental and numerical investigation reported for the laminar low-pressure premixed methane flame with and without benzene (1.5%).⁵

3. Experimental Section

Temperature and species mole fraction profiles have been measured in laminar stoichiometric premixed CH₄/O₂/N₂ and CH₄/1.5%C₆H₅CH₃/O₂/N₂ flames. Flame conditions are given in Table 1. Details on the experimental setup used in this work have been presented previously,^{5,36} and only its main features are briefly reviewed here. The flames were stabilized above a water-cooled porous plug flat flame burner. Chemical species

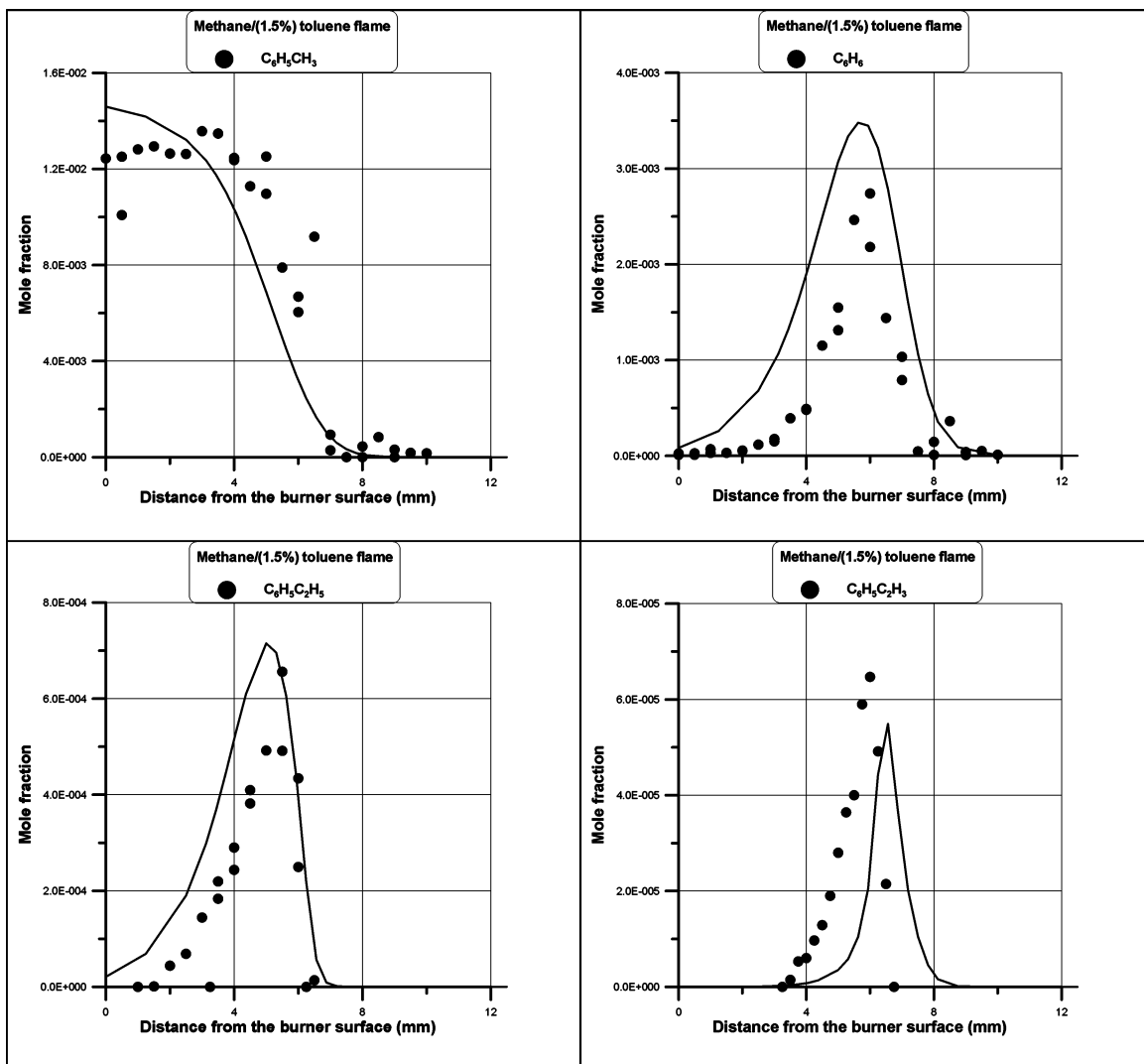


Figure 2. Comparison of computed (lines) and measured (symbols) mole fraction profiles of toluene, benzene, ethylbenzene, and styrene in CH₄/1.5% C₆H₅CH₃/O₂/N₂ flame at 0.0519 bar. $\phi = 1.0$.

were sampled by a deactivated 60° quartz cone with an orifice diameter of about 100 μm and form a molecular beam passing through three differentially pumped stages delimited by the sampling cone, the skimmer, and the collimator, respectively. The molecular beam is ionized by electron impact and analyzed by a quadrupole mass spectrometer. After mass discrimination, the signal is amplified by a second electron multiplier and an electrometer. The output is then fed to a phase sensitive amplifier for background signal subtraction. When it is possible, the ion source parameters are set to avoid strong fragmentation effects perturbing the flame composition profiles and/or to discriminate species of the same m/e . The mass spectrometer calibration is performed using the usual cold gas procedure for most stable species, the conservation of the total number of atoms of H₂O, and the pseudo-equilibrium method in the burnt gases for H, O, and OH. The stable species were also analyzed by gas chromatography (GC-FID/TCD) and by gas chromatography/mass spectrometry (GC/MS). The experimental error on the mole fraction of stable species was estimated to be about $\pm 10\%$. The mole fractions of all stable species presented in this paper were obtained by gas chromatography (GC-FID/TCD and GC/MS) except for H₂O and phenol, which were measured by using MB/MS. Temperature profiles were obtained by using a coated Pt/Rh(6%)–Pt/Rh(30%) thermocouple of 100 μm in diameter located 200 μm upstream from the cone tip. Conduction heat

losses were avoided by setting the thermocouple in a plane perpendicular to the laminar flow. Radiative heat was corrected by using the electric compensation method. Errors in the peak temperatures were estimated to be ± 100 K.

4. Reaction Mechanism and Species Properties

To simulate experimental mole fractions profiles measured in low-pressure methane/O₂/N₂ and methane/1.5% toluene/N₂ flames, the PC2A_mech1 mechanism recently published has been used.⁵ The mechanism PC2A_mech1 includes (i) GDF-Kin2.0 mechanism,³⁶ (ii) a submechanism of aromatic oxidation, and (iii) the low-temperature mechanism of Curran et al.²⁷

4.1. Methane Oxidation Submechanism. To model the oxidation of methane, the GDF-Kin2.0 mechanism,³⁶ a detailed mechanism optimized in very large conditions for natural gas oxidation, has been used. This mechanism includes the oxidation of minor and major alkanes (methane, ethane, propane, iso- and *n*-butane, *n*-pentane, and *n*-hexane) of the natural gas composition. The mechanism GDF-Kin2.0 was validated in a wide range of combustion regimes, including jet stirred reactor, shock tube, and premixed flames. Details are given in ref 36.

4.2. Aromatic Oxidation Submechanism. Benzene Oxidation. The submechanism describing the oxidation of benzene has been discussed in detail in our recent article.⁵ It includes

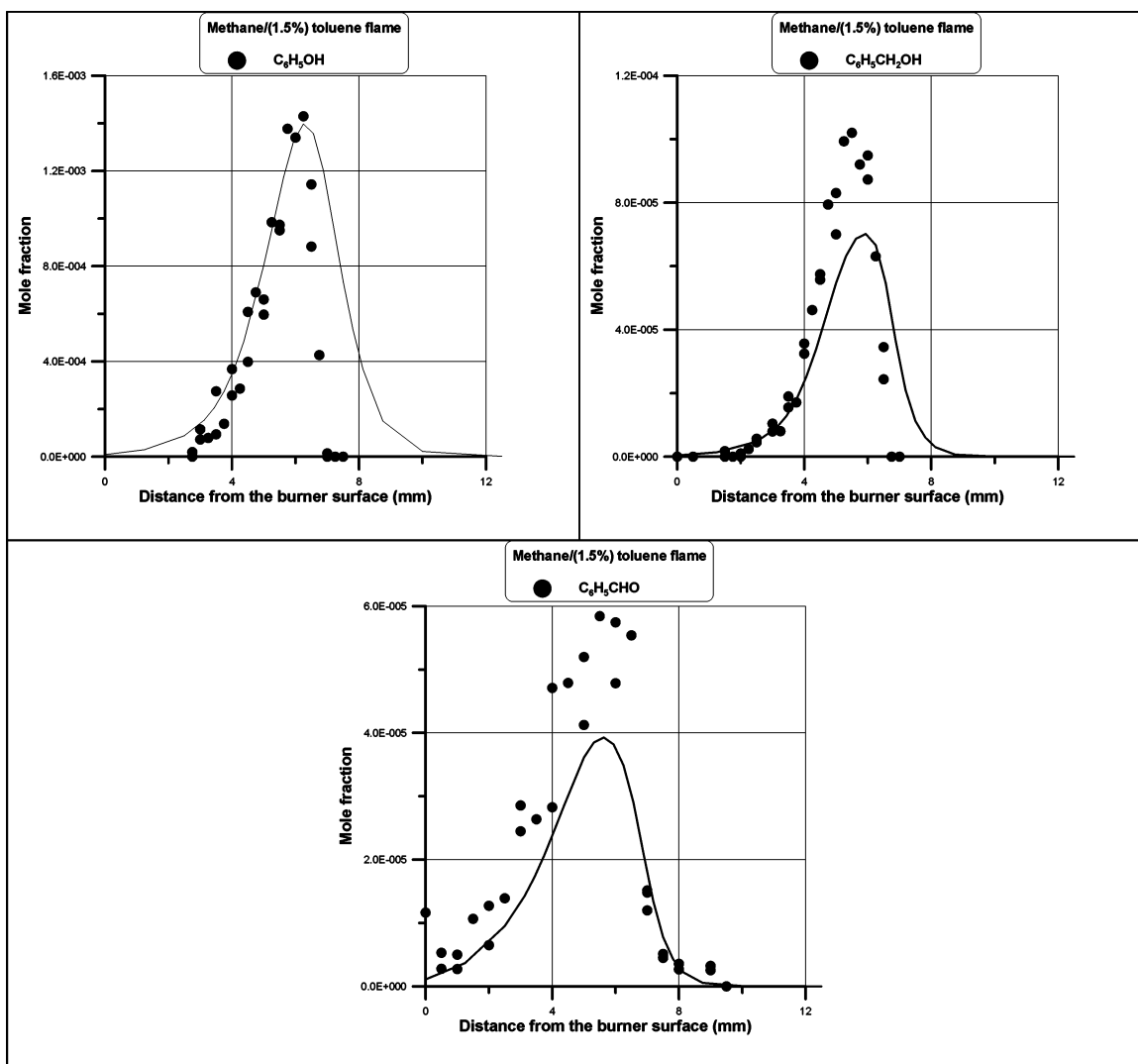


Figure 3. Comparison of computed (lines) and measured (symbols) mole fraction profiles of phenol, benzyl alcohol, and benzaldehyde in $\text{CH}_4/1.5\% \text{C}_6\text{H}_5\text{CH}_3/\text{O}_2/\text{N}_2$ flame at 0.0519 bar. $\phi = 1.0$.

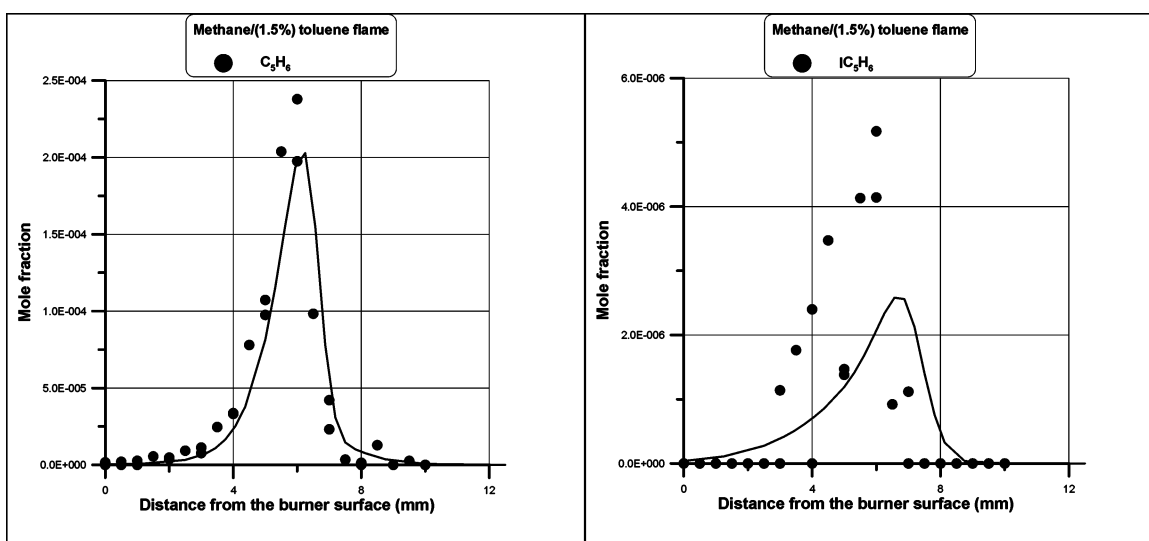


Figure 4. Comparison of computed (lines) and measured (symbols) mole fraction profiles of cyclopentadiene and pent-1-ynyl-3-ene in $\text{CH}_4/1.5\% \text{C}_6\text{H}_5\text{CH}_3/\text{O}_2/\text{N}_2$ flame at 0.0519 bar. $\phi = 1.0$.

the main reaction routes proposed in the literature except the reaction yielding *p*-benzoquinone ($\text{C}_6\text{H}_5 + \text{O}_2 = \text{C}_6\text{H}_4\text{O}_2 + \text{H}$). The chemistry of *p*-benzoquinone is not well-known; it was

postulated by Tan and Franck³⁷ to interpret the high concentration of H-atom measured in their investigation. The inclusion of this reaction led to a high computed concentration of

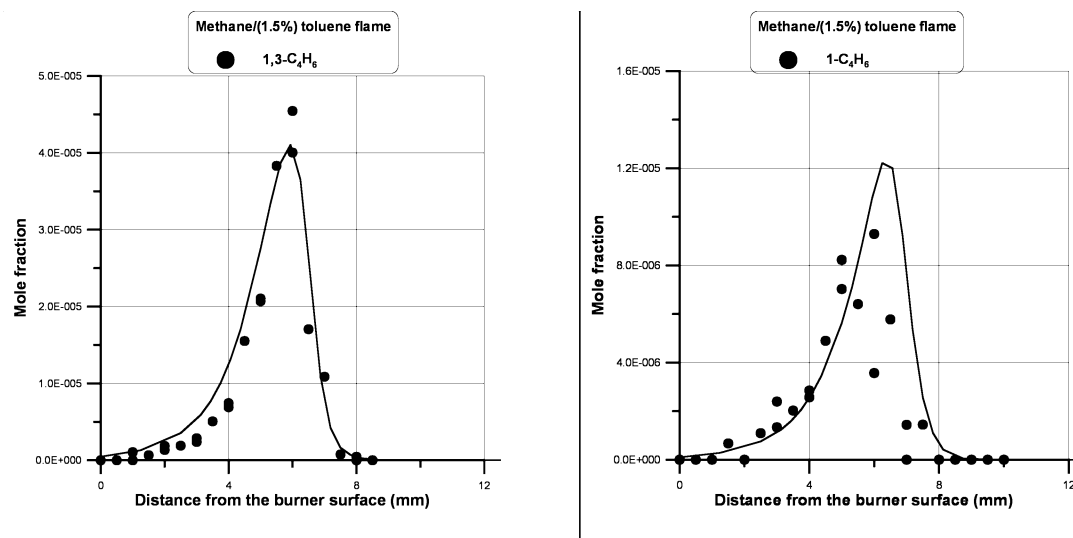


Figure 5. Comparison of computed (lines) and measured (symbols) mole fraction profiles of 1,3-butadiene and 1-butyne in CH₄/1.5% C₆H₅CH₃/O₂/N₂ flame at 0.0519 bar. $\phi = 1.0$.

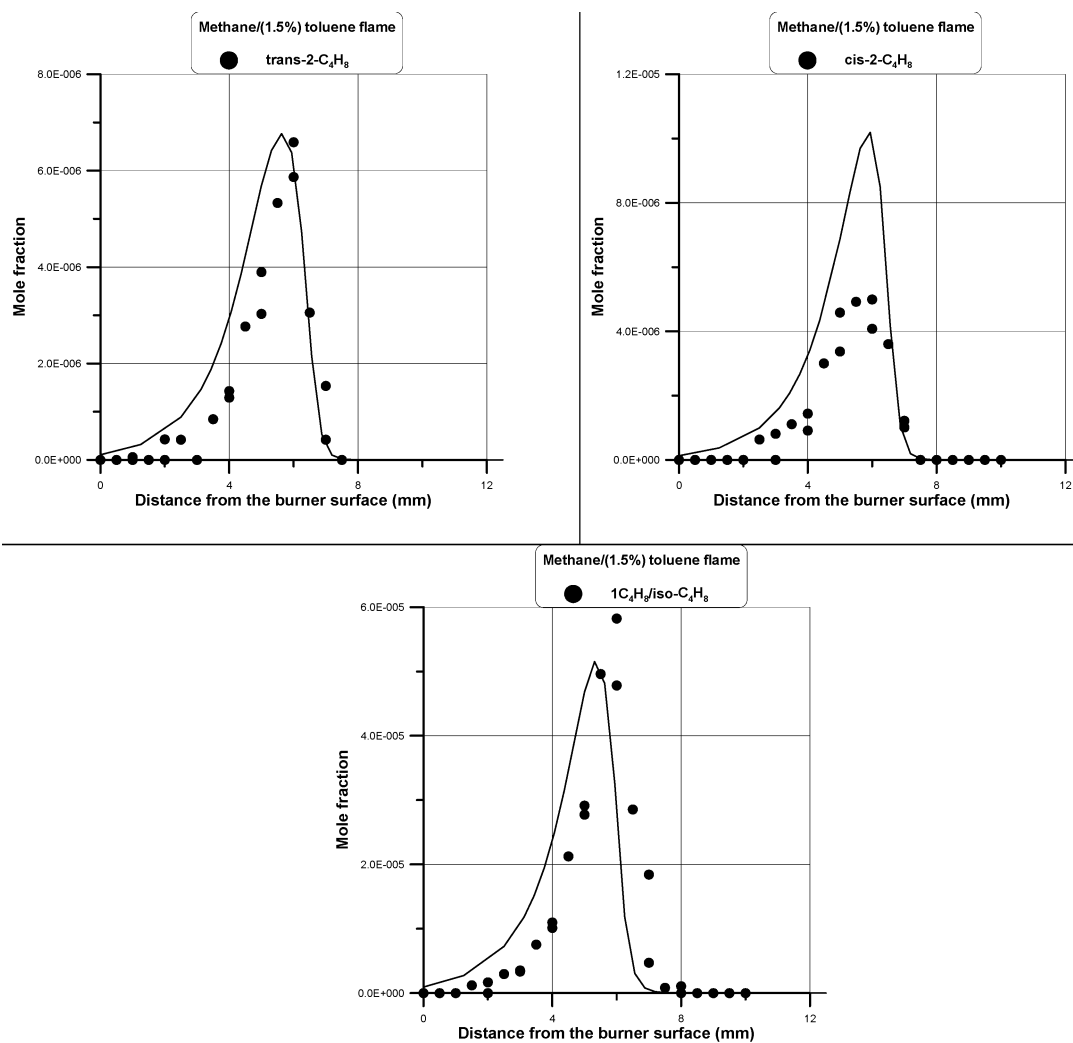


Figure 6. Comparison of computed (lines) and measured (symbols) mole fraction profiles of *trans*-2-butene, *cis*-2-butene, and the sum of 1-butene and isobutene in CH₄/1.5% C₆H₅CH₃/O₂/N₂ flame at 0.0519 bar. $\phi = 1.0$.

p-benzoquinone, whereas it was not detected experimentally by Tan and Franck³⁷ and in our experiments. Moreover, the main channel proposed by Tan and Franck³⁷ for the consumption of *p*-benzoquinone leads to CO and cyclopentadi-

none (C₅H₄O), and then cyclopentadienone concentration reaches a high value, whereas it was not detected in our methane–benzene and methane–toluene flames. The additional channels proposed by Wang³⁸ for *p*-benzoquinone depletion

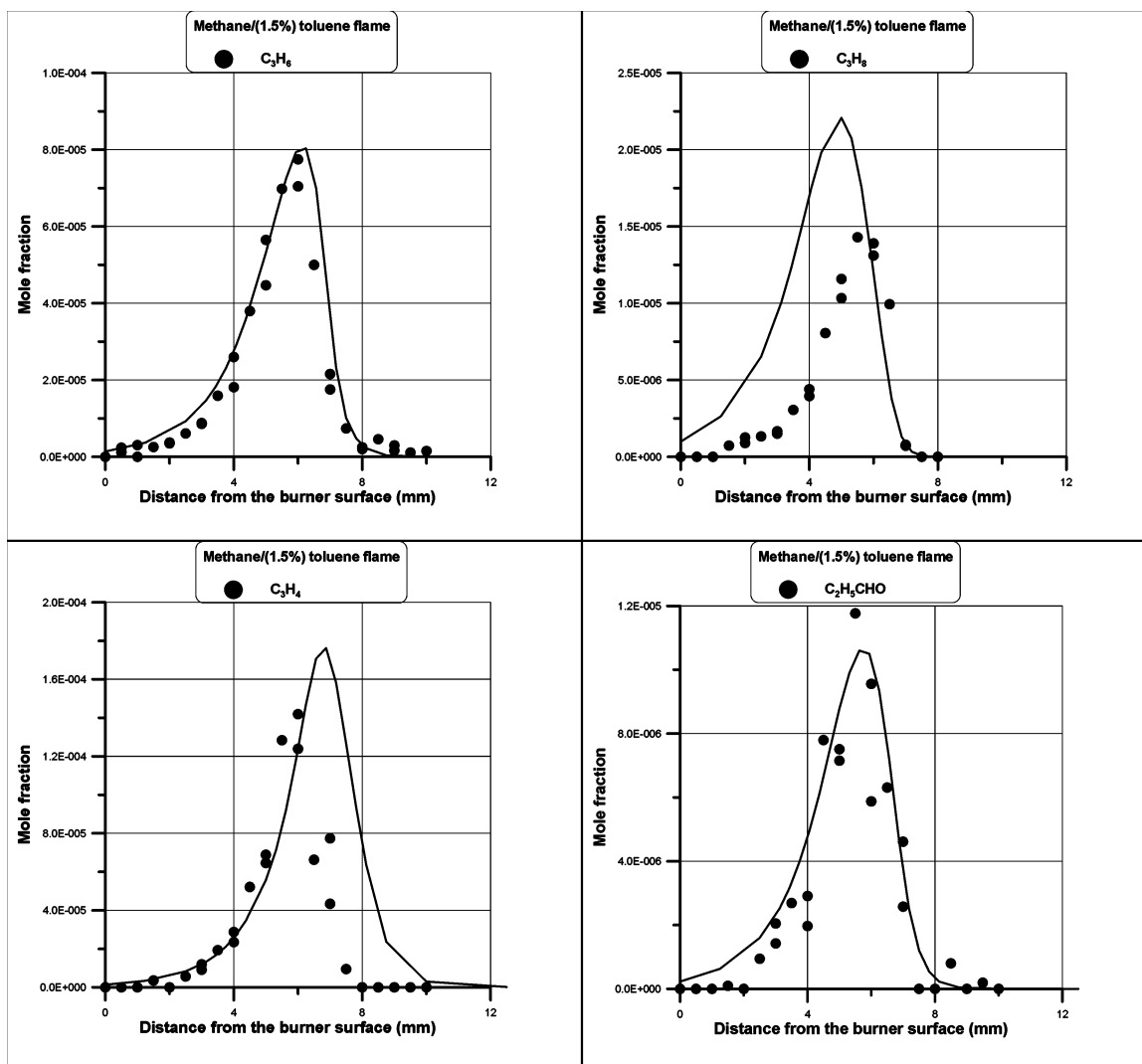
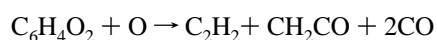
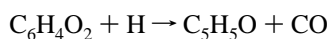


Figure 7. Comparison of computed (lines) and measured (symbols) mole fraction profiles of propene, propane, the sum of allene and propyne, and propanal in $\text{CH}_4/1.5\% \text{C}_6\text{H}_5\text{CH}_3/\text{O}_2/\text{N}_2$ flame at 0.0519 bar. $\phi = 1.0$.

by O and H radicals



have been tested and did not suppress the above observations. More details about the submechanism of benzene can be found in ref 5.

Toluene Oxidation Submechanism. The mechanism of Lindstedt and Maurice³¹ was preferred and included to our house mechanism. The mechanism of Lindstedt and Maurice³¹ for the oxidation of toluene has been validated in premixed and diffusion flame conditions. It has been also tested against detailed data obtained in reactors. Comparatively to the kinetic scheme outlined by Brezinsky¹³ for small aromatics, additional channels were proposed for the ring destruction. These channels are more probable to take place in flame conditions. However, some modifications were necessary to fit our present and previous experimental data. These slight changes concerned kinetic parameters of some reactions and will be systematically indicated in the next section. Moreover the mechanism postulated by Lindstedt and Skevis (LS),³³ which has largely inspired the mechanism of Lindstedt and Maurice,³¹ is supported by our experimental results. Indeed, pent-1-yn-3-ene (C_5H_6), which

is proposed in the LS model, was identified in methane/1.5% toluene and in methane 1.5% of *p*-xylene flames.

Note that, recently, to simulate the ignition delays of *n*-heptane/benzene mixtures measured at low temperature and high pressure in rapid compression machine, a submechanism of *n*-heptane for low- and high-temperature oxidation was incorporated to the mechanism PC2A_mech1. This submechanism derived from the model developed by Curran et al.²⁷ for *n*-heptane oxidation and was validated in a large range of parametric conditions. The details about this submechanism incorporated can be found in ref 5.

The final version of the mechanism used in this work (PC2A_mech1) is exactly the same to that one used to model $\text{CH}_4/\text{O}_2/\text{N}_2$ and $\text{CH}_4/1.5\% \text{C}_6\text{H}_6/\text{O}_2/\text{N}_2$ low-pressure flames. It comprises 627 species and 3074 elementary reactions (most of them are reversible). The mechanism including the references for the kinetic parameters and the thermodynamic and transport databases are available from the authors at the following e-mail address: abderrahman.el-bakali@univ-lille1.fr.

5. Results and Discussion

5.1. Temperature Profiles. Experimental temperature profiles measured by Pt/Rh (6%)–Pt/Rh (30%) thermocouple in methane and methane/1.5% toluene flames are shown in Figure 1. Both

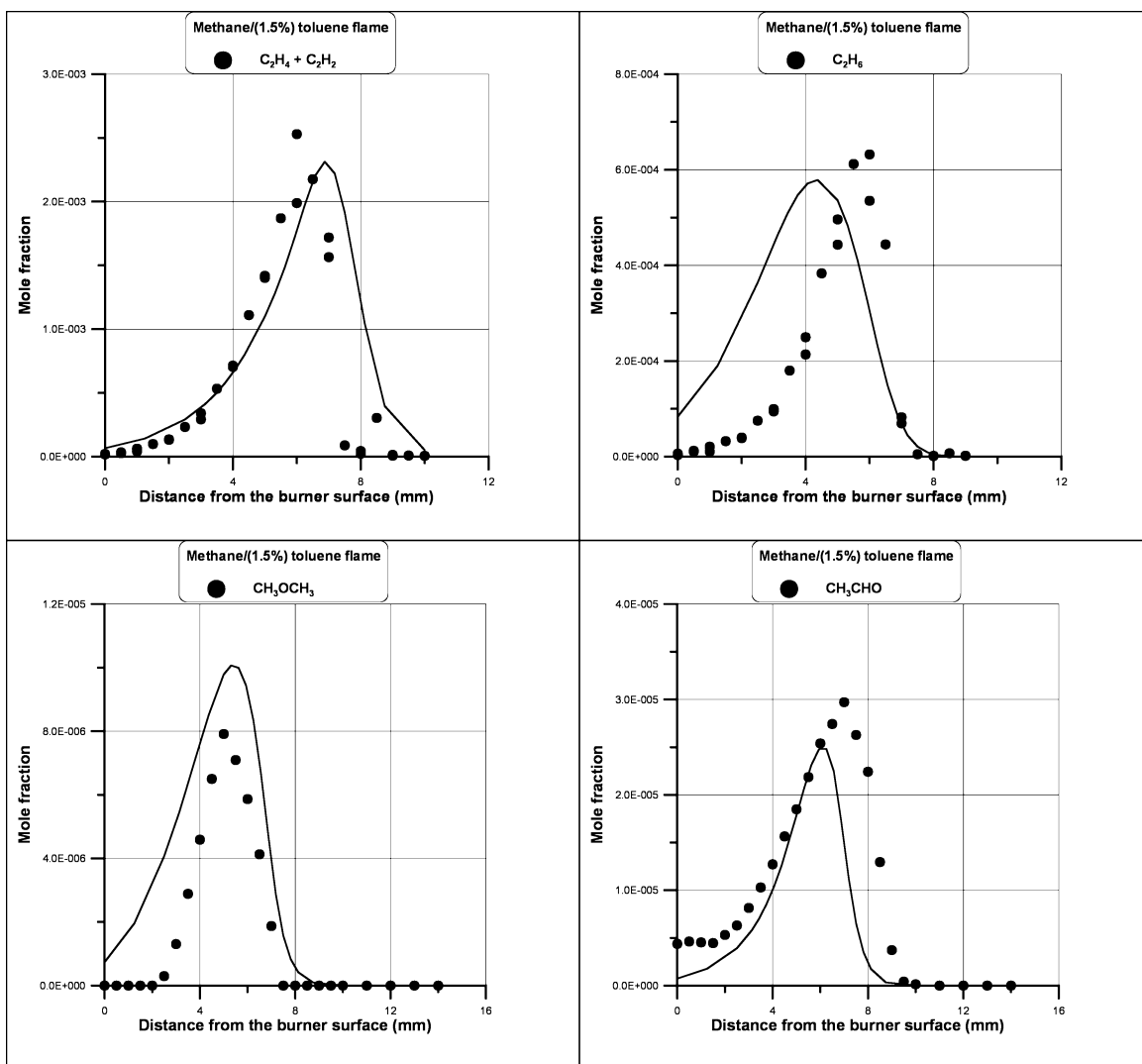
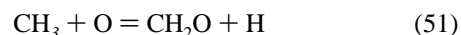


Figure 8. Comparison of computed (lines) and measured (symbols) mole fraction profiles of the sum of ethylene and acetylene, ethane, dimethyl ether, and acetaldehyde in CH₄/1.5% C₆H₅CH₃/O₂/N₂ flame at 0.0519 bar. $\phi = 1.0$.

profiles are corrected from radiation losses. The correction amounted to some 200 K in the burned gases. Both flames exhibit similar temperature profiles, and the peak temperatures measured for methane and methane–toluene flames are respectively 1603 and 1597 K. These peak values are lower than the adiabatic peak temperature because of heat losses mainly due to a water-cooled porous plug flat flame burner. Note that temperature profiles have been measured in the sampling conditions. This condition is required to ensure that sampling is performed at the same position where the temperature is measured. The similarity of temperature profiles indicates that the chemical structure of methane flame is not perturbed by the presence of toluene due to its low quantity. Therefore, it is expected that the methane–toluene system is kinetically mainly governed by methane oxidation.

5.2. Mole Fraction Profiles Species Obtained in the Methane Flame. Agreements between model predictions and experimental mole fractions for species produced by methane oxidation have been already presented and discussed in refs 4 and 5. Only the mean features of that work are briefly discussed in this paper. The agreement between the model and experiments is good for most species analyzed in this flame. The reaction path analysis identified hydrogen abstraction from methane to be the only significant consumption route of

methane. H-abstraction reactions proceed by H and OH and produce methyl radical CH₃. In these conditions, the consumption of methyl is governed exclusively by oxidation with oxygen atom:



Formaldehyde CH₂O produced in reaction 51 is depleted by hydrogen abstraction to formyl radical HCO mainly via reactions with H and OH. HCO undergoes thermal decomposition to form CO (HCO (+M) = CO + H (+M) (27)) which is exclusively converted to CO₂ via CO + OH = CO₂ + H (23).

The larger hydrocarbon species produced in the stoichiometric methane flame are propane C₃H₈, propene C₃H₆, ethane C₂H₆, ethyl radical C₂H₅, and ethylene C₂H₄. The main reaction responsible for these larger species formation is the self-recombination of methyl radicals to form ethane. Ethane is then mainly consumed by H-abstraction reactions with H, OH, and O, yielding ethyl radical which recombines with methyl to form propane. Propane depletion is controlled by H-abstraction reactions with OH and H to produce isopropyl and *n*-propyl radicals. The thermal decomposition of both radicals governs the formation of ethylene in our conditions. Isopropyl radical loses hydrogen atom, yielding propene.

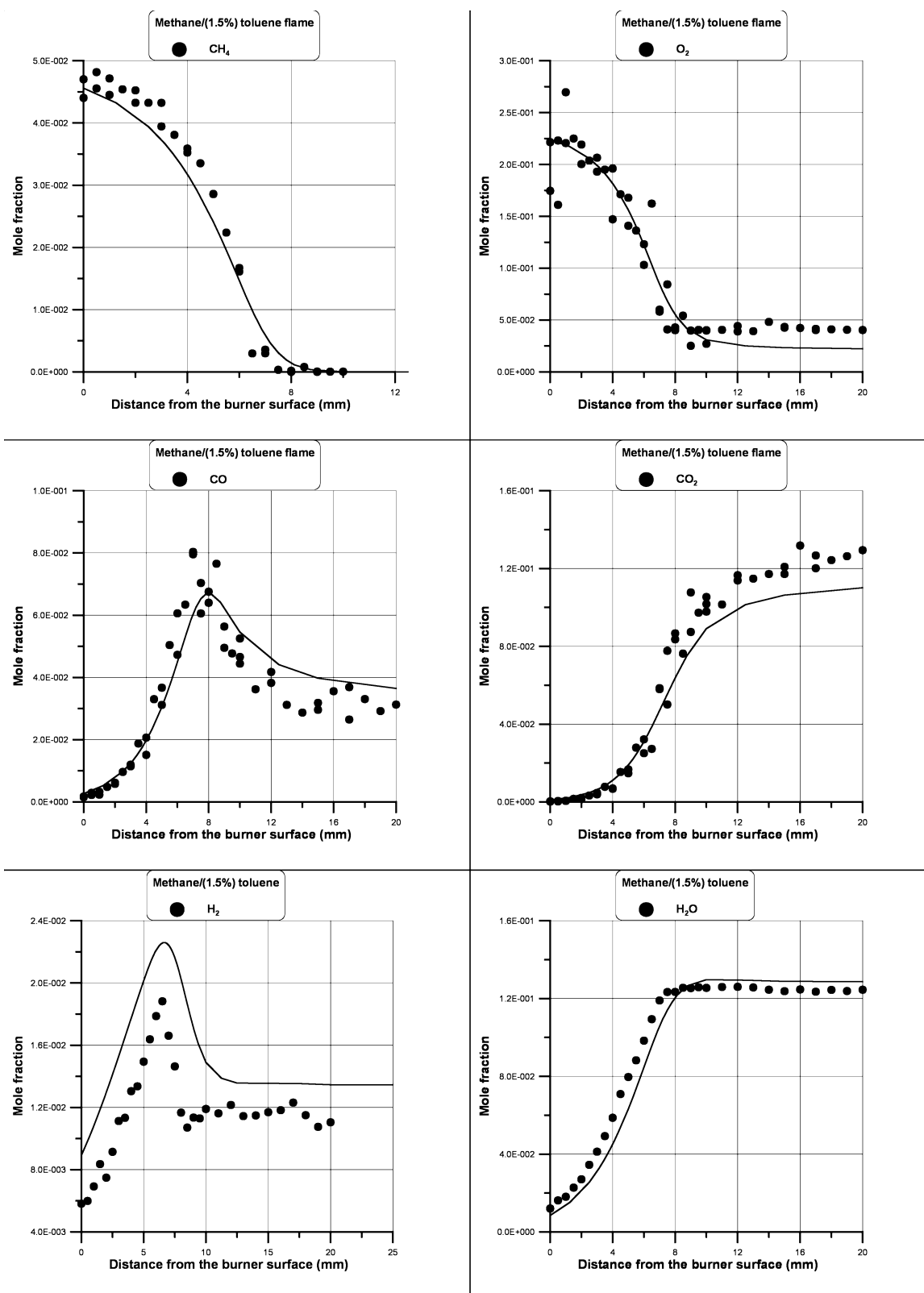


Figure 9. Comparison of computed (lines) and measured (symbols) mole fraction profiles of methane, O_2 , CO , CO_2 , H_2 , and H_2O in $CH_4/1.5\%C_6H_5-CH_3/O_2/N_2$ flame at 0.0519 bar. $\phi = 1.0$.

5.3. Mole Fraction Profiles of Species Measured in the Methane/Toluene Flame. Mole fraction profiles of reactants (methane, toluene, and molecular oxygen), final products (carbon monoxide, carbon dioxide, molecular hydrogen, and water), and reactive (H , O , and OH) and stable ($C_2H_4 + C_2H_2$, C_2H_6 , C_3H_6 , C_3H_8 , $1-C_4H_8 + i-C_4H_8$, and cis and trans $2-C_4H_8$, $1,3-C_4H_6$, $1-C_4H_6$, and C_5H_6) intermediate aliphatic species have

been analyzed. Oxygenated hydrocarbon species detected in a significant concentration were acetaldehyde CH_3CHO , dimethyl ether CH_3OCH_3 , and propanal C_2H_5CHO . In addition to toluene, the main aromatic species analyzed are benzene, phenol, ethylbenzene, benzyl alcohol, styrene, and benzaldehyde.

The comparison of computed and experimental mole fractions for all species analyzed in the methane-toluene flame are shown

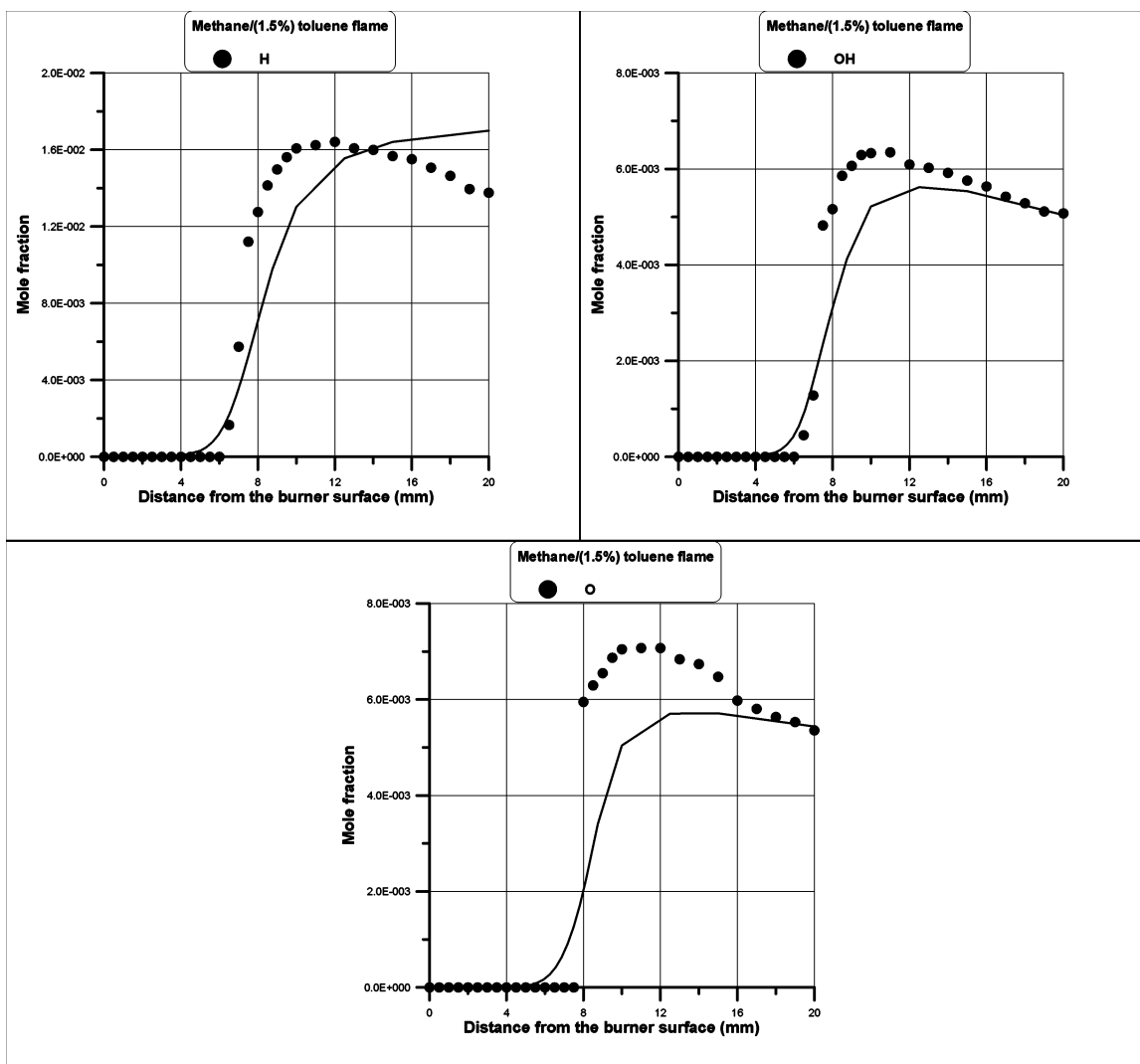
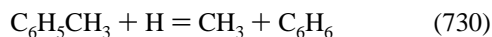


Figure 10. Comparison of computed (lines) and measured (symbols) mole fraction profiles of active species H, OH, and O in CH₄/1.5% C₆H₅-CH₃/O₂/N₂ flame at 0.0519 bar. $\phi = 1.0$.

in Figures 2–10. Globally, the model predicts correctly these new experimental data.

Toluene Depletion. The consumption of toluene is well-predicted by the model (Figure 2). However, the model overestimates the mole fraction of toluene close to the burner surface. Modeling indicates that toluene is mainly consumed by H-abstraction reactions with H and OH and by elimination of methyl, involving hydrogen atom (Figure 11):



The rate constants proposed by Baulch et al.³⁹ were assigned to the above reactions. The H-abstraction reactions with oxygen atom is not effective, and the elimination of hydrogen with larger abstractors like methyl and HO₂ radicals was observed to be negligible due the large activation energy for these reactions.

The three electrophilic addition of oxygen atom reactions were included in the mechanism, and only the reaction yielding *p*-methylphenoxy radical OC₆H₄CH₃ participates in toluene depletion (Figure 11). For this reaction, kinetic parameters reported by Hoffman et al.⁴⁰ were used.

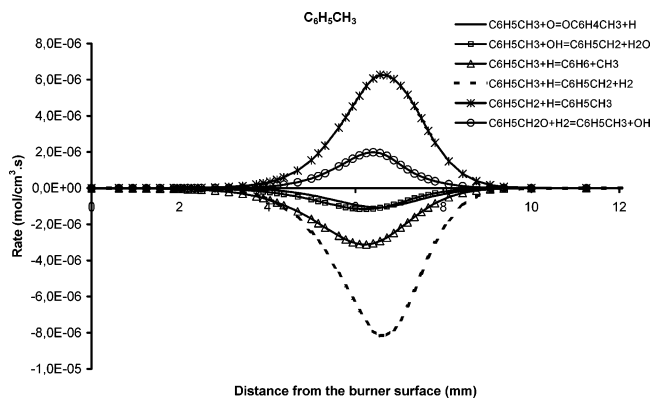


Figure 11. Rates of production of toluene in a stoichiometric methane/air/1.5% toluene flame.

The unimolecular thermal decomposition of toluene yielding methyl and phenyl radicals ($\text{C}_6\text{H}_5\text{CH}_3 = \text{CH}_3 + \text{C}_6\text{H}_5$) supported by many shock tube investigations^{41,42} was observed to be not a significant route of toluene consumption in our conditions because the reverse reaction ($\text{CH}_3 + \text{C}_6\text{H}_5$) is faster.

Benzyl radical was not detected experimentally in this work. As can be seen from Figure 12, benzyl radical is principally formed by H-abstraction reactions from toluene with H and OH.

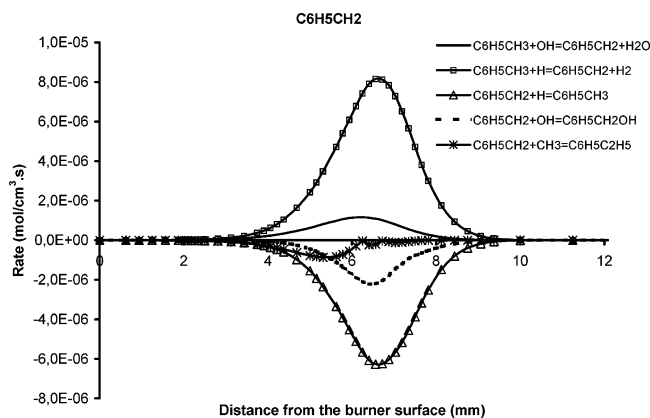


Figure 12. Rates of production of benzyl radical in a stoichiometric methane/air/1.5% toluene flame.

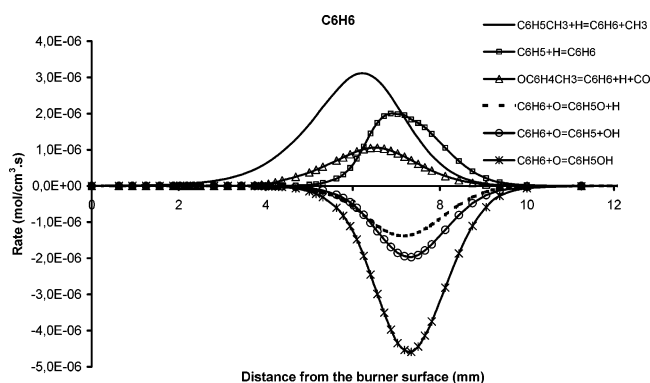
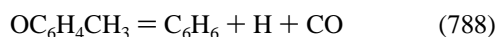
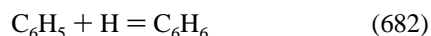
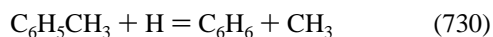


Figure 13. Rates of production of benzene in a stoichiometric methane/air/1.5% toluene flame.

However, the reaction of benzyl radical with H atom is faster and governs its consumption:

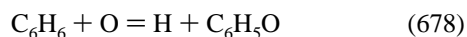


Since reaction 732 occurs with a high rate, toluene depletion via benzyl radical formation is moderated and occurs with a rate similar to the route producing benzene and methyl. Therefore, according to our analysis, benzene should be the major stable primary product of the toluene consumption. Indeed, our experimental data show benzene to be the largest mole fraction intermediate aromatic species. Figure 2 shows that a very good agreement is observed between the computed and the experimental mole fraction profiles of benzene. Modeling indicates that benzene formation is governed by the following reactions (Figure 13):

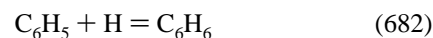


The rate constants used for reactions 730 and 788 were proposed by Baulch et al.³⁹ and Lin and Lin,⁴³ respectively.

The main reactions involved in the consumption of benzene are (i) H-abstraction reactions with oxygen atom yielding phenyl and (ii) O-oxidation reactions yielding phenol or phenoxy radical:

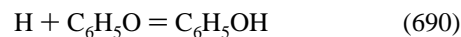


Phenyl radical mainly produced by the previous reactions (675) and $\text{C}_6\text{H}_5\text{C}_2\text{H}_3 + \text{H} = \text{C}_6\text{H}_5 + \text{C}_2\text{H}_4$ (-812) is then consumed by recombination reaction with H-atom (682) and by its oxidation by O_2 (680), yielding respectively benzene and phenoxy radical (Figure 14):



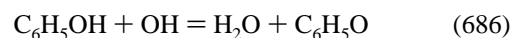
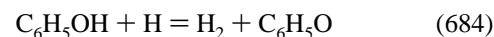
Phenyl and phenoxy were not detected in our experimental conditions. The stoichiometric methane flame was seeded with a small quantity of toluene (1.5%), and the chemistry is dominated by the CH_4/O_2 system. However, phenol was analyzed and predicted by the model with very good accuracy, as shown in Figure 3.

The formation of phenol occurs via reaction 676 and the recombination reaction of H-atom with phenoxy (Figure 15):



Reaction 690 converts phenoxy radical to phenol at moderate temperature. At high temperature, due to the activation energy, the reverse reaction yielding phenoxy becomes more effective.

The consumption of phenol is dominated by H-atom abstraction reactions with active species H and OH:



Reactions 684 and 686 are the most important source of phenoxy radical. As shown in Figure 16, phenoxy radical is also formed by oxidation of phenyl radical by O_2 (678) and by addition of O-atom on benzene (680). It is mainly consumed by the thermal decomposition reaction 688, yielding cyclopentadienyl (C_5H_5) and CO. The reaction of recombination of phenoxy with H-atom to form phenol (690) contributes to its destruction at moderate temperature.

According to our modeling, the oxidation of toluene in our conditions is mainly controlled by the submechanism of benzene oxidation discussed in detail in our previous article.⁵ However, due to the high quantity of methyl radical present in the methane-toluene flame, the route involving benzyl radical is also significant. Indeed, the nonconverted mole fraction of benzyl radical to toluene by reacting with H is responsible for most larger alkyl aromatic compounds analyzed in this work. The chemical kinetics of benzyl radical are not known, and most kinetic parameters reported in the literature have been proposed to fit experimental data. The shock tube investigation of Hippler et al.⁴⁴ concluded that there is no evidence for benzyl radical to react with molecular oxygen. However, the investigation of Fenter et al.,⁴⁵ conducted at low temperature, reported that peroxy adduct exists below 600 K and disappears at moderate temperature (1000 K). Note that the investigation of Hippler et al.⁴⁴ has been performed in the 1200–1500 K temperature range. The reaction of benzyl with molecular oxygen yielding *p*-methylphenoxy $\text{OC}_6\text{H}_5\text{CH}_3$, was included in our mechanism, and the rate constant of Brezinsky et al.¹² was considered. Davis and Law¹⁰ studied the reaction of benzyl radical with HO_2 and suggested a benzylhydroperoxide as the intermediate adduct. This reaction is also considered in the model with the rate constant of Hippler et al.⁴⁴ The kinetic parameters determined by Davis

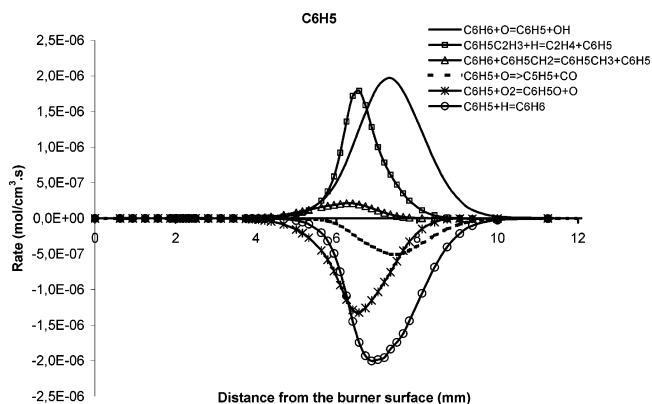


Figure 14. Rates of production of phenyl radical in a stoichiometric methane/air/1.5% toluene flame.

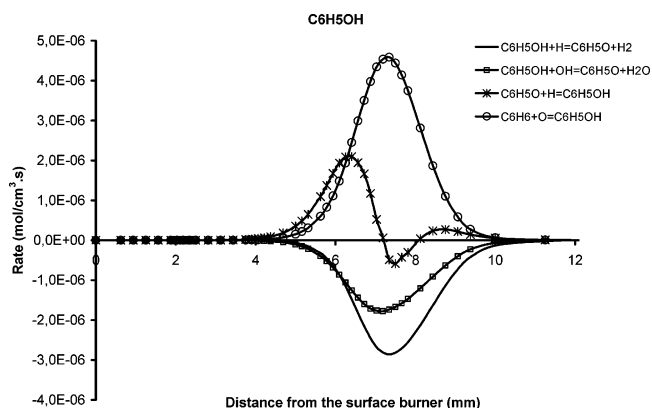


Figure 15. Rates of production of phenol in a stoichiometric methane/air/1.5% toluene flame.

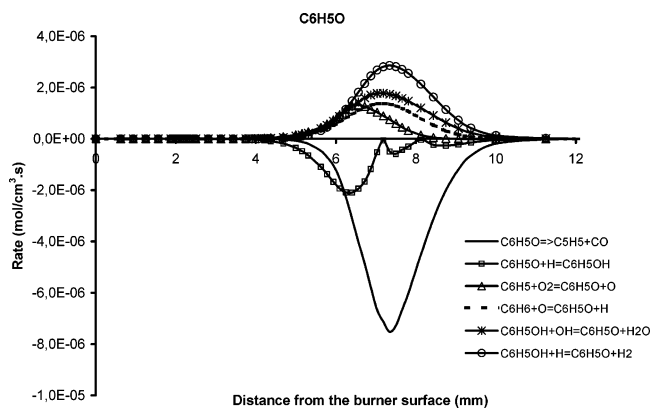


Figure 16. Rates of production of phenoxy in a stoichiometric methane/air/1.5% toluene flame.

and Law¹⁰ correspond to the high-pressure limit rate coefficient for adduct dissociation.

According to our calculations (Figure 12), three radicals react significantly with benzyl radical: methyl, OH, and O. These reactions are responsible for alkyl and oxygenated aromatic compounds formation observed in our conditions. The reaction with methyl radical takes place due to the high methyl mole fraction in the methane–toluene flame:



The rate constant for this reaction comes from Colket and Seery.⁴⁶ The presence of methane favors the formation of larger alkyl aromatics (Figure 2). Indeed reaction 818 initiates the

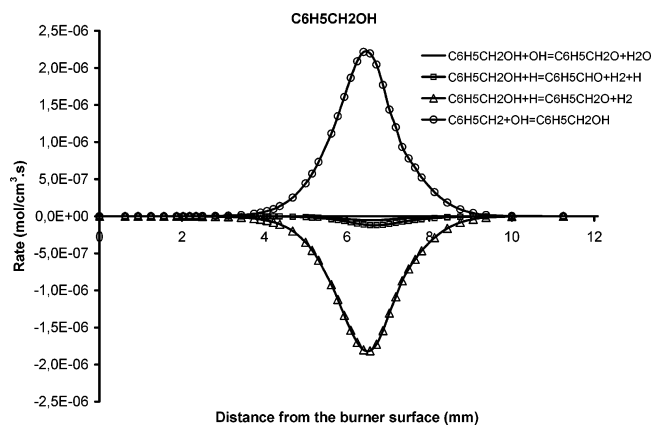


Figure 17. Rates of production of benzyl alcohol in a stoichiometric methane/air/1.5% toluene flame.

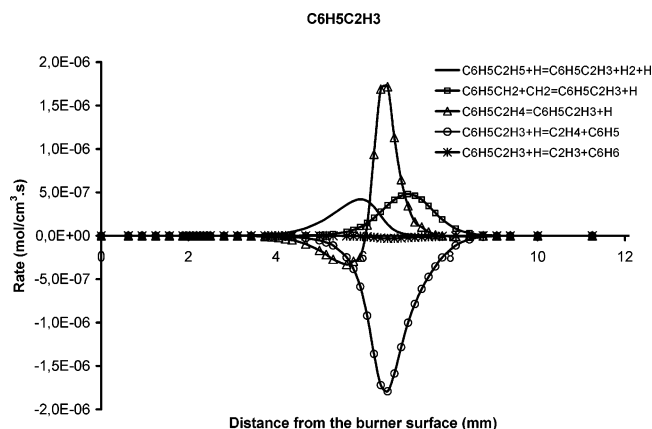
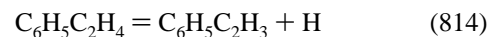


Figure 18. Rates of production of styrene in a stoichiometric methane/air/1.5% toluene flame.

formation of various alkyl aromatics. It is the main source of ethylbenzene C₆H₅C₂H₅. Ethylbenzene is mainly consumed by the thermal decomposition yielding 1-phenylethyl radical C₆H₅C₂H₄:



The 1-phenylethyl radical thermal decomposition was found to be the major source of styrene C₆H₅C₂H₃ in our conditions (Figure 2):



The recombination of benzyl and methylene radicals also contributes to styrene formation (Figure 18):



Styrene reacts with H-atom, yielding ethylene and phenyl radical:



Three oxygenated aromatic species have been experimentally observed: benzyl alcohol C₆H₅CH₂OH, benzaldehyde C₆H₅CHO, and phenol C₆H₅OH. Figure 3 compares their computed and experimental mole fractions for the three species. The agreement between the model and experiment is excellent for phenol and good for benzaldehyde and benzyl alcohol.

Figure 17 shows that benzyl alcohol C₆H₅CH₂OH is kinetically controlled by two reactions. It is issued from OH addition

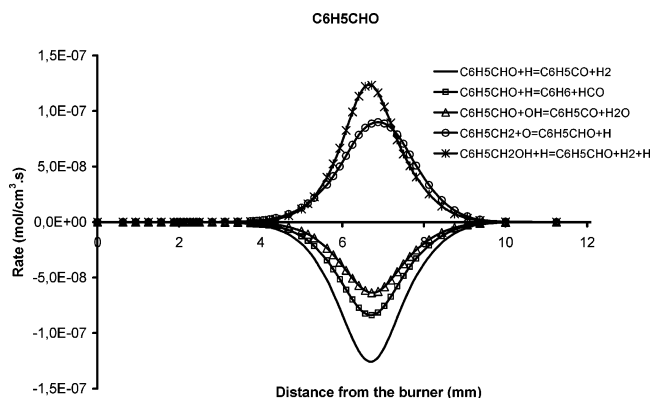


Figure 19. Rates of production of benzaldehyde in a stoichiometric methane/air/1.5%toluene flame.

on the benzyl radical and reacts exclusively with H-atom to produce benzoyl radical $C_6H_5CH_2O$:

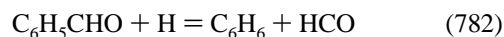


Benzaldehyde is mainly formed by the reaction of benzyl with oxygen atom (748) and of benzyl alcohol with H (774):



The best agreement for benzaldehyde was obtained by assigning the rate coefficients of Baulch et al.³⁹ to this reaction. Pitz et al.²⁵ also reported that reaction 748 with Baulch's rate coefficients was essential for modeling shock tube experiments.

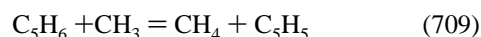
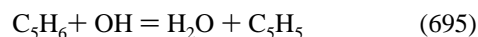
Figure 19 shows that benzaldehyde depletion in the methane–toluene flame mainly proceeds via the following reactions, yielding benzene or benzoyl radical C_6H_5CO :



Benzoyl radical decomposes to form phenyl and carbon monoxide:



The formation of cyclopentadiene C_5H_6 is a key route in the aromatic oxidation. The comparison of the computed and experimental mole fraction for cyclopentadiene, presented in Figure 4, shows very good agreement. The evolution of cyclopentadiene is connected to the cyclopentadienyl radical C_5H_5 via the following reactions:



The formation of C_5H_5 predominantly proceeds via reaction 693 and the thermal decomposition of phenoxy radical C_6H_5O :



The C_5H_5 radical is significantly consumed by recombination with H atom and its isomerization, yielding the corresponding linear species IC_5H_5 :

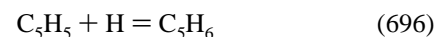
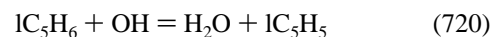
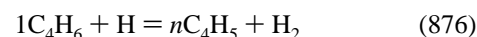
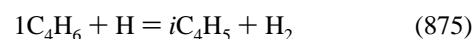
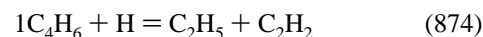
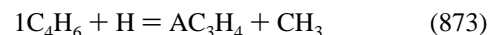


Figure 4 shows that the agreement is not good between computed and experimental mole fraction profile for pent-1-ynyl-3-ene IC_5H_6 ; the model under-predicts the experiment. The chemistry of IC_5H_6 is connected to C_5H_5 radical and it still not well-known. Nevertheless, the analysis of this species in the present work supports the model proposed by Linsdstedt and Skevis³³ for benzene oxidation at atmospheric pressure: the formation of pent-1-ynyl-3-ene mainly occurs from cyclopentadiene and cyclopentadienyl via IC_5H_5 . In our low-pressure methane–toluene flame, IC_5H_6 is mainly produced by the reaction $nC_3H_4 + CH_3 = IC_5H_6$ (−721) and is consumed by H-abstraction reactions involving O and OH:



5.4. C_4 Hydrocarbon Species. Two isomeric forms of C_4H_6 , buta-1,3-diene and but-1-yne, have been observed experimentally. The agreement between the modeling and the experimental results for these species is very good (Figure 5). The formation and consumption of both species are governed by routes similar to that observed in the methane–benzene flame.⁵ But-1,3-diene (C_4H_6) is mainly formed by the recombination of vinyl radicals, $C_4H_6 = 2C_2H_3$ (−174), whereas but-1-yne ($1C_4H_6$) is produced by the recombination of propargyl radical with CH_3 through $C_3H_3 + CH_3 = 1C_4H_6$ (879). But-1,3-diene is essentially consumed via reaction $C_4H_6 + OH = nC_4H_5 + H_2O$ (431) and by its thermal decomposition reaction at high temperature, $C_4H_6 = 2C_2H_3$ (−174). But-1-yne is consumed via the following H-atom abstraction/addition reactions:



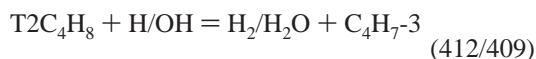
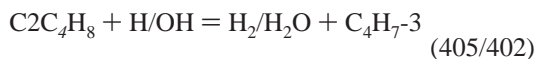
Isomers of C_4H_8 (but-1-ene, isobutene, and *cis*- and *trans*-but-2-ene) were detected in the methane–toluene flame. But-1-ene ($1C_4H_8$) and isobutene (iC_4H_8) were not analyzed separately; the sum of their mole fractions is correctly predicted by the model (Figure 6).

As mentioned for the methane–benzene flame,⁵ the formation of butenes is largely controlled by C_3H_5 and CH_3 recombination:



The butenes were not observed in the reference flame (methane flame) due to the low C_3H_5 concentration. Indeed, the main

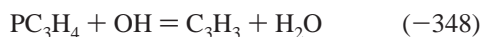
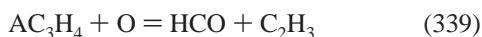
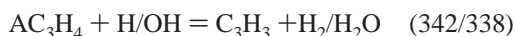
source of C₃H₅ radicals is propene, which is more produced in the methane–toluene flame (see the next section). Butenes are consumed exclusively by H-abstraction reactions with H, O, and OH. These reactions produce isobutenyl (*i*C₄H₇) or but-1-en-3-yl (C₄H₇₋₃) radicals:



5.5. C₃ Species: C₃H₄ (Allene/Propyne), Propene, and Propane. Allene and propyne were observed experimentally exclusively in the CH₄/1.5% C₆H₅CH₃/O₂/N₂ flame (Figure 7). These species were not distinguished experimentally; the modeled and measured profiles shown in Figure 7 correspond to the sum of allene and propyne, and good agreement was observed.

Allene formation occurs mainly by H-abstraction of allyl radical AC₃H₅ with H-atom: AC₃H₅ + H = AC₃H₄ + H₂ (314), whereas propyne is exclusively formed via the recombination of C₃H₃ with H-atom.

Allene depletion involves H, O, and OH, while O atom does not contribute to propyne destruction:

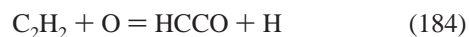


Propene C₃H₆ was analyzed in both methane and methane–toluene flames. It was found that the addition of toluene significantly increases the mole fraction peak of C₃H₆. As shown in Figure 7, this effect is excellently captured by the model. The recombination of vinyl and methyl radicals is the major source of propene in the methane–toluene flame. The same route controls the formation of propene in the methane flame, but it occurs with a slow rate due to the low quantity of vinyl radicals produced in these conditions. As discussed above for methane flame, the thermal decomposition of propan-2-yl radical *i*-C₃H₇, formed from propane, contributes to propene formation: *i*-C₃H₇ + M = C₃H₆ + H + M (−297). Propene depletion proceeds mainly by H-atom abstraction by H: C₃H₆ + H = H₂ + AC₃H₅ (298).

5.6. C₂ Species: Ethane and Acetylene + Ethylene. C₂ species have been analyzed in both flames: ethane and the sum of acetylene and ethylene mole fractions. The sum of the modeled and experimental mole fractions of acetylene and ethylene are presented in Figure 8, and very good agreement is observed. Figure 8 also compares the prediction of the model with experiment for ethane. The addition of toluene to methane flame decreases the ethane quantity and significantly increases the total peak mole fraction of C₂H₂ + C₂H₄. Both experimental observations are well-captured by the model (Figure 8). Ethane

decrease is due to the methane decrease in the methane–toluene flame. Methane is the major source of methyl radical which in turn is the main source of ethane by its self-recombination.

According to our calculations, acetylene is the major olefin formed in our conditions. In the methane–toluene flame, acetylene is produced by the reaction IC₅H₅ = C₃H₃ + C₂H₂ (717). The thermal decomposition of the linear C₅H₅ species takes place exclusively in the methane–toluene flame. In addition to reaction 717, acetylene formation is favored due to the high vinyl mole fraction produced in the seeded flame. Indeed, additional reactions produce vinyl in the flame blends via the sequence C₅H₅ → *n*C₄H₅ → C₂H₃, which enhances reaction −158, C₂H₃ (+M) = C₂H₂ + H (+M), in the CH₄/1.5%toluene/O₂/N₂ flame. Acetylene depletion occurs by oxidation with oxygen atom:



5.7. C₁ Species, Major Species, and Burnt Gas Active Species (H, O, OH). The consumption of methane and molecular oxygen is well-predicted by the model (Figure 9). Methane depletion proceeds mainly via H-abstraction reaction by H-atom:



Due to the higher initial concentration of methane in the seeded flame, reaction 41 is more effective in the reference flame. Consequently, methyl radical, which issued mainly from reaction 41, is less formed in the methane–toluene flame.

The main products analyzed in both flames were CO, H₂, H₂O, and CO₂. As can be seen from Figure 9, their mole fraction profiles are correctly predicted by the model except the mole fraction of H₂ which is slightly overestimated. The experimental results show an increase of CO and CO₂ mole fractions and a decrease of H₂ and H₂O. These observations are directly due to the initial quantity of carbon and H atoms which varies when methane is partially replaced by toluene. Keeping the global equivalence ratio constant, the initial mole fraction of carbon increases and the mole fraction of H decreases in the seeded flame. Even if the decrease of CO in the seeded flame is largely due to the decrease of the initial quantity of carbon, reaction path analyses identified the elimination of CO by phenoxy radical as a nonnegligible reaction in CO formation: C₆H₅O ⇒ CO + C₅H₅ (688). However, CO₂ is exclusively formed by the reaction CO + OH = CO₂ + H (23).

The reactive species H, O, and OH have been also measured in this work, and as can be seen from Figure 10, the model reasonably predicts their evolution. Note that H and OH were observed lower in the seeded flame due to the higher H/C ratio in the reference flame.⁵

Comparatively to the benzene–methane flame, the low-pressure methane–toluene flame operating at stoichiometric conditions produces various alkyl aromatic species such as ethylbenzene, styrene, benzaldehyde, and benzenyl alcohol. Our simulations point out that benzyl radical and the abundance of methyl radical favor alkyl aromatic formation. In the stoichiometric methane–benzene flame, this route is negligible due to the low mole fraction of toluene formed. However, toluene depletion in the methane flame via benzene formation was identified to be responsible for more than 50% of toluene degradation in our conditions. These simulations are in agreement with the experimental results; benzene and phenol were

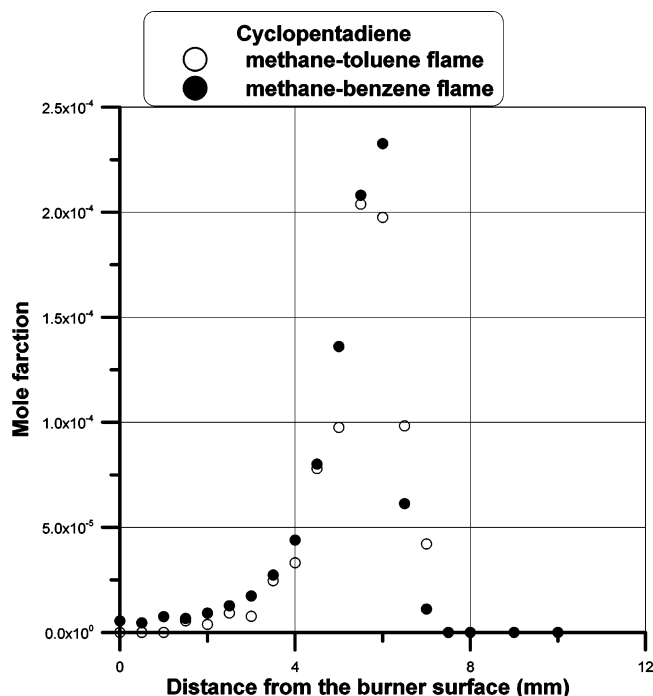


Figure 20. Experimental mole fraction profiles of cyclopentadiene measured in stoichiometric methane/air/1.5% benzene and methane/air/1.5% toluene flames.

observed as the major stable intermediate aromatic species in the methane–toluene flame.

Another interesting point concerns the similarity observed for aliphatic species in methane flame with 1.5% benzene or 1.5% toluene; in both flames similar mole fraction profiles have been observed for allene, propyne, isomers of C_4H_8 , buta-1,3-diene, and but-1-yne. Note that these species have been observed exclusively in the seeded flames. Moreover, similar effects of toluene and benzene addition on acetylene, ethylene, and propene mole fractions have been observed. These observations support a similar kinetic scheme of benzene and toluene degradation in methane low-pressure stoichiometric flames. Reaction path analyses show that benzene oxidation occurs via phenoxy radical, which undergoes thermal degradation yielding cyclopentadienyl radical whose chemistry is directly connected to cyclopentadiene. In the case of the methane–toluene flame, the main depletion way for toluene occurs via the formation of benzene and phenol, which yields phenoxy. On the other hand, the oxidation sequence of the alkyl aromatic issued from benzyl radical finally converges to phenoxy, which in turn exclusively produces cyclopentadienyl and CO.

As discussed in ref 5 for the methane–benzene flame, the above-mentioned aliphatic species are issued from cyclopentadiene depletion. Cyclopentadiene was also found responsible of the significant increase of the intermediate species mole fraction (acetylene/ethylene, propene) analyzed in the methane flame with and without 1.5% toluene. Figure 20, shows that similar experimental mole fraction profiles have been analyzed in the methane–benzene and methane–toluene flames. This experimental observation clearly supports (i) the convergence of toluene and benzene oxidation sequences to cyclopentadienyl radical and (ii) the key role of cyclopentadiene in aliphatic formation.

Conclusions

Experimental mole fraction profiles of stable and unstable species have been measured in laminar stoichiometric premixed

$CH_4/O_2/N_2$ and $CH_4/1.5\%C_6H_5CH_3/O_2/N_2$ flames at low pressure (0.052 atm) by using MB/MS and GC-MS techniques. Temperature profiles were measured with a coated Pt/Rh thermocouple in the sampling conditions. It was observed that toluene addition does not affect the temperature profile. However, the mole fraction of aliphatic species (acetylene + ethylene, propene) analyzed in both flames increases significantly in the seeded flame with toluene. Moreover, various species have been observed exclusively in methane–toluene flame, namely, allene + propyne, buta-1,3-diene, but-1-yne, but-1-ene + isobutene, *cis*- and *trans*-but-2-ene, cyclopentadiene, benzene, phenol, ethylbenzene, benzylalcohol, styrene, benzaldehyde, and toluene. Similar experimental observations have been recently reported in the case of methane–benzene flame, except for aromatic species. Indeed, only phenol could be observed in methane/1.5% benzene flame.

A recently developed detailed kinetic mechanism was used to model these new experimental results, and good agreement between the model and experiments has been observed. The kinetic mechanism has been also used for the assessment of major reaction pathways in both flames. Reaction pathways responsible for the formation and consumption of selected species were identified by means of the analysis of their rates of production. It was found that toluene depletion mainly proceeds via benzene ($C_6H_5CH_3 + H = C_6H_6 + CH_3$) or benzyl radical formation ($C_6H_5CH_3 + H = C_6H_5CH_2 + H_2$), both contributing almost equally to toluene destruction in a stoichiometric methane–toluene flame. As reported for benzene–methane flame, benzene oxidation rapidly leads to phenoxy radical in the methane–toluene flame. Benzyl radicals react with methyl and OH to produce alkyl aromatics whose oxidation sequence is ended by phenoxy radical formation. Phenoxy undergoes a unimolecular decay to yield cyclopentadienyl radicals and CO. Cyclopentadienyl radicals were observed highly connected to cyclopentadiene. It is clearly shown by the reaction paths analysis that both benzene and toluene depletion in a seeded stoichiometric methane flame converges to cyclopentadiene via formation of phenoxy radical. As the experimental mole fraction profiles of cyclopentadiene were observed to be similar and as the reaction kinetic mechanism for its oxidation is identical in both flames, benzene or toluene addition produces similar aliphatic species with similar concentration.

References and Notes

- (1) Dagaut, P.; El Bakali, A.; Ristori, A. *Fuel* **2006**, *85*, 944.
- (2) Frenklach, M. *Phys. Chem. Chem. Phys.* **2002**, *4*, 2028.
- (3) Simmie, J. *Prog. Energy Combust. Sci.* **2003**, *29*, 299.
- (4) Dupont, L.; El Bakali, A.; Pauwels, J. F.; Da Costa, I.; Meunier, P.; Richter, H. *Combust. Flame* **2003**, *135*, 171.
- (5) El Bakali, A.; Ribaucour, M.; Saylam, A.; Vanhove, G.; Therssen, E.; Pauwels, J. F. *Fuel* **2006**, *85*, 881.
- (6) Burcat, A.; Farmer, R. C.; Espinoza, R. L.; Matula, R. A. *Combust. Flame* **1979**, *36*, 313.
- (7) Burcat, A.; Snyder, C.; Brabbs, T. *NASA Technical Memorandum TM-87312*; National Aeronautical and Space Administration: Washington, DC, 1986.
- (8) Roubaud, A.; Minetti, R.; Sochet, L. R. *Combust. Flame* **2000**, *121*, 535.
- (9) Davis, S. G.; Wang, H.; Brezinsky, K.; Law, C. K. *Proc. Combust. Inst.* **1996**, *26*, 1025.
- (10) Davis, S. G.; Law, C. K. *Combust. Sci. Technol.* **1998**, *140*, 427.
- (11) Venkat, C.; Brezinsky, K.; Glassman, I. *Proc. Combust. Inst.* **1982**, *19*, 143.
- (12) Brezinsky, K.; Litzinger, T. A.; Glassman, I. *Int. J. Chem. Kinet.* **1984**, *16*, 1053.
- (13) Brezinsky, K. *Prog. Energy Combust. Sci.* **1986**, *12*, 1.
- (14) Emdee, L. J.; Brezinsky, K.; Glassman, I. *J. Phys. Chem.* **1992**, *96*, 215.
- (15) Ristori, A.; Dagaut, P.; Pengloan, G.; El Bakali, A.; Cathonnet, M. *Combustion* **2001**, *1*, 265.

- (16) McLain, A. G.; Jachimowski, C. F.; Wilson, C. H. *NASA Technical Paper 1472*; National Aeronautical and Space Administration: Washington, DC, 1979.
- (17) Asaba, T.; Fujii, N. *Proc. Combust. Inst.* **1971**, *13*, 155.
- (18) Fujii, N.; Asaba, T. *Proc. Combust. Inst.* **1973**, *14*, 155.
- (19) Bittker, D. A. *NASA Technical Memorandum TM-100202*; National Aeronautical and Space Administration: Washington, DC, 1987.
- (20) Bittker, D. A. *Combust. Sci. Technol.* **1991**, *79*, 49.
- (21) Lovell, A. D.; Brezinsky, K.; Glassman, I. *Proc. Combust. Inst.* **1988**, *20*, 1063.
- (22) He, Y. Z.; Mallard, W. G.; Tsang, W. J. *Phys. Chem.* **1988**, *92*, 2196.
- (23) Bittker, D. A. *NASA Technical Paper 3546*; National Aeronautical and Space Administration: Washington, DC, 1995.
- (24) Klotz, S. D.; Brezinsky, K.; Glassman, I. *Proc. Combust. Inst.* **1998**, *27*, 337.
- (25) Pitz, W. J.; Seiser, R.; Bozzelli, J. W.; Da Costa, I.; Fournet, R.; Billaud, F.; Battin Leclerc, F.; Seshadri, K.; Westbrook, K. Joint Meeting of the U.S. Sections of the Combustion Institute, 2nd, March, 2001.
- (26) Zhong, X.; Bozzelli, J. W. *J. Phys. Chem. Sci.* **1998**, *102*, 13537.
- (27) Curran, H.; Gaffuri, P.; Pitz, W. J.; Westbrook, W. *Combust. Flame* **1998**, *114*, 149.
- (28) Bozzelli, J.; Sebbar, N.; Pitz, W. J.; Bockhorn, H. Joint Meeting of the U.S. Sections of the Combustion Institute, 2nd, March, 2001.
- (29) Dagaut, P.; Pengloan, G.; Ristori, A. *Phys. Chem. Chem. Phys.* **2002**, *4*, 1846.
- (30) Sivaramakrishnam, R.; Tranter, R. S.; Brezinsky, I. *Proc. Combust. Inst.* **2004**, *30*, 9400.
- (31) Lindstedt, R. P.; Maurice, L. Q. *Combust. Sci. Technol.* **1996**, *120*, 119.
- (32) Shandross, R.; Longwell, J. P.; Howard, J. B. *Proc. Combust. Inst.* **1996**, *26*, 711.
- (33) Lindstedt, R. P.; Skevis, G. *Combust. Flame* **1994**, *99*, 551.
- (34) Zhong, X.; Mckinon, J. T. *Combust. Sci. Technol.* **1995**, *107*, 261.
- (35) Hamins, A.; Seshadri, K. *Combust. Flame* **1987**, *68*, 295.
- (36) El Bakali, A.; Dagaut, P.; Pillier, L.; Desgroux, P.; Pauwels, J. F.; Rida, A.; Meunier, P. *Combust. Flame* **2004**, *137*, 109.
- (37) Tan, Y.; Franck, P. *Proc. Combust. Inst.* **1996**, *26*, 677.
- (38) Wang, H. *Prepr. Symp.—Am. Chem. Soc., Div. Fuel Chem.* **1998**, *43*, 113.
- (39) Baulch, D. L.; Cobos, C. J.; Cox, R. A.; Esser, C.; Franck, P.; Just, Th.; Pilling, M. J.; Troe, J.; Walker, R. W.; Warnatz, J. *J. Phys. Chem. Ref. Data* **1992**, *21*, 2.
- (40) Hoffman, A.; Klatt, M.; Wagner, H. *Gg. Z. Phys. Chem.* **1990**, *168*, 1.
- (41) Pamidimukalla, K. M.; Kern, R. D.; Patel, M. R.; Wei, H. C.; Kiefer, J. H. *J. Phys. Chem.* **1987**, *91*, 2148.
- (42) Rao, V. S.; Skinner, G. B. *J. Phys. Chem.* **1989**, *93*, 1864.
- (43) Lin, C. Y.; Lin, M. C. *J. Phys. Chem.* **1986**, *90*, 425.
- (44) Hippler, H.; Reihls, C.; Troe, J. *Proc. Combust. Inst.* **1990**, *33*, 37.
- (45) Fenter, F. F.; Noziere, B.; Caralp, F.; Lesclaux, R. *Int. J. Chem. Kinet.* **1994**, *26*, 171.
- (46) Colket, M. B.; Seery, D. *Proc. Combust. Inst.* **1994**, *25*, 883.